Acta Neuropathologica Communications

RESEARCH

Open Access

Spatial analysis of a complete DIPG-infiltrated brainstem reveals novel ligand-receptor mediators of tumour-to-TME crosstalk

Anja Kordowski[1*], Onkar Mulay[1,3], Xiao Tan[1,3], Tuan Vo[3,8,9], Ulrich Baumgartner[2], Mellissa K. Maybury[4], Timothy Hassall[5,6], Lachlan Harris[1,2,7], Quan Nguyen[1,3] and Bryan W. Day[1,2,5*]

Abstract

Previous studies have highlighted the capacity of brain cancer cells to functionally interact with the tumour microenvironment (TME). This TME-cancer crosstalk crucially contributes to tumour cell invasion and disease progression. In this study, we performed spatial transcriptomic sequencing analysis of a complete annotated tumour-infiltrated brainstem from a single diffuse intrinsic pontine glioma (DIPG) patient. Gene signatures from ten sequential tumour regions were analysed to assess mechanisms of disease progression and oncogenic interactions with the TME. We identified four distinct tumour subpopulations and assessed respective ligand-receptor pairs that actively promote DIPG tumour progression via crosstalk with endothelial, neuronal and immune cell communities. Our analysis found potential targetable mediators of tumour-to-TME communication, including members of the complement component system and the neuropeptide/GPCR ligand-receptor pair *ADCYAP1-ADCYAP1R1*. These interactions could influence DIPG tumour progression and represent novel therapeutic targets.

Keywords DIPG, Spatial transcriptomic sequencing, Tumour-CNS crosstalk, Ligand-receptor pairs, *ADCYAP1-ADCYAP1R1*

*Correspondence:
Anja Kordowski
Anja.Kordowski@seattlechildrens.org
Bryan W. Day
Bryan.Day@qimrberghofer.edu.au
[1]Queensland Institute for Medical Research, Brisbane, QLD 4006, Australia
[2]School of Biomedical Sciences, The University of Queensland, Brisbane, QLD 4067, Australia
[3]Institute for Molecular Bioscience, The University of Queensland, Brisbane, QLD 4067, Australia
[4]Child Health Research Centre, The University of Queensland, Brisbane, QLD 4101, Australia
[5]Children's Brain Cancer Centre, UQ Frazer Institute, Brisbane, QLD 4102, Australia
[6]Queensland Children's Hospital, Brisbane, QLD 4101, Australia
[7]School of Biomedical Sciences, Queensland University of Technology, Brisbane, QLD 4059, Australia
[8]Hunter Medical Research Institute, Precision Medicine Research Program, Newcastle, NSW 2305, Australia
[9]School of Biomedical Sciences and Pharmacy, The University of Newcastle, Newcastle, NSW 2308, Australia

Introduction

Ongoing spatially-resolved sequencing technologies offer unprecedented possibilities to study cellular functionality and organisation. The necessity to understand healthy and diseased tissues in its entirety becomes even more evident for the human brain, the most complex organ of the body. The brain's cellular architecture and corresponding functions are tightly regulated. However, in the presence of central nervous system (CNS) pathologies, such as brain tumours, this intercellular network is disrupted. More importantly, brain cancer cells form a part of this network and build unique microenvironmental interconnections [1, 2]. H3 K27-altered diffuse midline Gliomas (DMGs), are a family of aggressive paediatric brain cancers with no curative treatment options and are most commonly found in the pontine region of the

brainstem, where they are termed diffuse intrinsic pontine glioma (DIPG). These tumours affect children at an approximate median age of 6 to 7 years, with the majority succumbing to disease within one year [3, 4]. Major disease obstacles include intratumoural genetic and cellular heterogeneity as well as a highly invasive phenotype. The development of promising targeted therapies for DIPG has long been hindered due to the lack of tumour tissue for laboratory research. Major efforts initiated by Monje and colleagues, established the first DIPG cell line and PDX animal model from patient autopsy tissue [5]. This success together with an increase of routinely performed stereotactic biopsies led to broad access to DIPG biopsy and autopsy specimens, which formed the basis of global research efforts that continue to grow today [5]. Major findings in the field include the identification of loss of histone H3 trimethylation, as well as subtype-specific amplifications and mutations [6–12]. These findings led to vital information that transformed DIPG treatment and classification [13]. Beyond the DIPG tumour mutational landscape, Filbin and colleagues shed light onto tumour cell-intrinsic properties and developmental programs of H3 K27-altered gliomas. Comprehensive sequencing analyses at the single cell level revealed that DMG tumours are largely comprised of oligodendrocyte precursor (OPC-like) cells that give rise to more differentiated astrocyte (AC-like)/mesenchymal (MES-like) and oligodendrocyte (OC-like) cell populations. Extended work by Liu et al. has shown that OPC-like populations can be further divided into more immature (OPC-like 2 and 3) and more committed OPC-like 1 states [14, 15]. Additionally, this study examined the architecture of these tumours at the single-cell spatial level, suggesting the presence of functionally distinct tumour niches.

Other studies investigated how glioma cells, including DIPG, take advantage of intercellular communication and actively integrate into TME networks. In the context of adult glioblastoma (GBM), Winkler and colleagues unravelled the complexity of these networks, demonstrating that intercellular communication is cell type-specific and that different glioma subpopulations functionally connect with each other in different ways [2]. Collectively, these discoveries emphasise the intricacy of intratumoural heterogeneity and the importance of understanding how glioma cells interact with the TME to promote pathogenesis.

The current study, in collaboration with the Queensland Children's Tumour Bank (QCTB) in Brisbane, collected fresh tumour tissue from a single mapped DIPG patient at autopsy, spanning the entire tumour-infiltrated brainstem from midbrain down to the spinal cord. Whilst numerous genetic studies on DIPG tumours from spatially distinct locations have been reported, analysis on wholly intact tissue remains sparse. To address this unmet need, we performed 10x Visium spatial transcriptomic sequencing on the ten sequential DIPG brainstem regions. We identified four different tumour cell populations in our dataset and performed ligand-receptor (LR) prediction analysis to assess how DIPG tumour communities interact with the TME. Our findings highlighted the importance of the vascular niche and the contribution of neuronal and myeloid cells to DIPG disease progression. Amongst others, our results suggest a role for the complement system as well as for the LR pair *ADCYAP1-ADCYAP1R1* in DIPG disease progression.

Materials and methods

Patient tissue sampling and ethical consideration

The DIPG tumour specimen used for this study was de-identified and obtained through the QCTB with consent of the patient's legal representative. The donation was collected within hours of the patient's death and spanned the entire brainstem, including midbrain, pons, medulla oblongata and upper spinal cord regions. Tissue pieces were collected from each region and subsequently formalin-fixed for the preparation of paraffin-embedded (FFPE) tissue blocks.

Immunohistochemistry (IHC)

FFPE tissue sections were deparaffinised, rehydrated and tissue epitopes masked during the FFPE process retrieved with a heat-induced method, using a pressure cooker and 10% [w/v] sodium citrate, pH 6.0. Tissues were stained, using the antihistone H3 (mutated K27M) antibody (abcam, ab240310) 1:200, anti-PACAP38 (abcam, ab216627) 1:50, anti-ADCYAP1R1 (LSBio, LS-B13181) 1:50, anti-NeuN (Merck, MAB377) 1:50 and Hoechst nuclear stain 1:10,000. Images were processed on the Aperio FL Slide Scanner. H&E (hematoxylin and eosin) staining was performed by the QIMRB Histology Core Facility and processed on the Aperio AT Turbo Brightfield Scanner.

RNA quality control of FFPE tissue blocks

The proportion of RNA fragments with a size of at least 200 nucleotides (DV200) was determined for all tissue samples prior to sequencing. 2x cuts a 10 µm per sample were collected and total RNA extracted using the RNeasy FFPE kit (QIAGEN). RNA concentration was determined on the Nanodrop and 50ng/µl used for DV200 indexing employing the Agilent Tapestation.

Tissue preparation, probe design and library constructions

Spatial transcriptomic sequencing was performed with the 10x Visium CytAssist Spatial Gene Expression platform for FFPE sections. Steps were followed according to the Visium CytAssist for FFPE sections User Guide. In brief, DIPG FFPE tissue blocks were rehydrated under

moist conditions in RNAse-free H_20 for 1 h at 4 °C prior to sectioning. FFPE blocks were cut at a thickness of 5 µm on a microtome. Sections were allowed to fully flatten in a 42 °C water bath and transferred onto a microscope glass slide. Slides were placed on a 42 °C hot plate for 3 h and further dried overnight in a glass jar containing desiccator beads. Tissue slides were deparaffinised, stained (H&E) and imaged according to standard histology workflows on day two. Upon imaging and chemical decrosslinking, the slides were placed into a Visium CytAssist Tissue Slide Cassette with a 6.5 × 6.5 mm gasket and prepared for probe hybridisation overnight. Probe ligation, release and extension were performed on the following day. A qPCR step was included to determine the PCR cycle number (C_q value) for sample indexing and cDNA amplification. Sample fragment size and sample quality were assessed accordingly for library constructions and sequencing.

Alignment and quality control (QC)

Raw FASTQ files were processed employing the SpaceRanger software and mapped to the human genome (hg38). Gene expression was quantified based on unique molecular identifier (UMI) counts. For QC adjustment, low quality spots with < 2,500 and > 75,000 gene counts were removed on each sample individually. The content of mitochondria genes was assessed, but not filtering applied.

Data analysis

All sequencing analyses were carried out using RStudio (v4.2.0) or Python (v3.8).

Data integration, spatially-informed clustering and cell type identification

The data of each sample was first merged and further integrated using the anchor-based data integration workflow (nfeatures = 3000, normalisation.method = SCTransform) from the Seurat package (v4.3.0) before unsupervised cell type identification was performed. Based on Clustree (v0.5.0), a resolution of 0.3 was used for clustering. Marker genes for each cell community were determined with the *FindAllMarkers* (only.pos = T, p_val_adj < 0.05) function and cell types identified, using the web-based intuitive enrichment analysis tool EnrichR [16].

CNV estimation for the prediction of tumour content

To identify evidence of large-scale chromosomal copy number variations (CNVs), the InferCNV package (v1.14.1) was utilised. The gene expression data from three human dorsolateral pre-frontal cortex (DLPFC) Sects. (151507, 151669, 151673), obtained from *spatialLIBD* [17] (https://bioconductor.org/packages/spatialLIBD) were used as a normal reference. The data from the ten DIPG sections and the three normal references was integrated as described above to generate a SeuratObject. With this, a grouped annotation file was provided according to normal or tumour sample (ref_group_names = section). The human genecode hg38 from TrinityCTAT was chosen as a gene order file providing the chromosomal location for each gene. CNV predictions were performed using the six-state Hidden Markov Model (HMM = T) with a specified threshold of 0.2 (BayesMaxPNormal = 0.2). The resulting metadata from the InferCNV object was added to the integrated spatialLIBD/DIPG SeuratObject for downstream analysis and plotting.

Conditional autoregressive-based deconvolution (CARD)

CARD was used to delineate spots with higher tumour content from spots that primarily contain normal cell types, and further to determine the degree of DIPG cellular states in the dataset. Single cell data from Filbin and colleagues, focussing on DMG cell states, was used as a reference (GSE184357) [15]. The CARD workflow was followed as described previously [18] and according to the GitHub tutorial, using the default settings.

Spatial trajectory interference, ligand-receptor (LR) and cell-cell interaction (CCI) analysis

Analysis of spatial trajectory interference, LR pairing and CCIs was conducted, using the Python-based software stLearn (v.0.4.12) as described previously [19]. Tissue sections from each region were analysed individually, filtered by parameters (min_genes = 3, min_cells = 100) and then normalised by library size. The processed data were analysed using the stLearn spatial trajectory inference algorithm, which reconstructs cellular trajectories within tissue sections by leveraging spatial distances, morphological features, and gene expression data. Community C6 was defined as the root, and the spatial distribution of communities C0, C1, C6 and C0 trajectories was thoroughly mapped to uncover cellular dynamics and interactions within the tissue context. LR co-expression profiling and equivalent expression levels (LR_{SCORE}) between neighbouring spots and between two cell types were based on the repository CellPhoneDB [20]. P-values for each spot and LR pair ($p_{s,\ LR}$) were used to calculate the CCI_{LR} matrices.

Data availability

The processed spatial transcriptomic sequencing data generated in this study is available through the GEO database, accession number GSE280990. All other files are available within the Supplementary Information provided with this paper.

Results

Patient case report and tumour classification

A male, aged 7 years and 7 months, presented as part of a general clinical investigation for a unilateral coloboma, with an incidental finding of a T2 and FLAIR hyperintense lesion (AP: 25 mm, TP: 22 mm, CC: 35 mm) involving the inferior pons and medulla dorsally (Fig. 1a.I). The patient displayed no specific signs of neurological deficit and remained well for a period of 6 years and 10 months with no imaging changes or indication of disease progression. 7.5 years after the initial scan, he had a presyncopal episode and reported new symptoms including headaches, increased slurring of speech and ataxia. MRI showed an infiltrative neoplastic lesion, demonstrating moderate interval progression of the pons and medulla with new involvement of the cerebellar peduncles (Fig. 1a.II). Histopathology and molecular profiling from stereotactic biopsy sampling diagnosed a diffuse midline glioma, H3 K27M mutant (*H3F3A* c83.A > T), MGMT unmethylated, with *TP53*, *ATRX* and *PPM1D* somatic point mutations and copy number variation loss of chromosome 5q, 15q and 18 (Table Fig. 1b). The patient received standard of care local field radiotherapy (RT) of 50 Gy in 30 fractions using a VMAT technique, resulting in no clinical improvement. MR imaging 5 months post RT demonstrated concerning disease progression (lesion size 35 × 43 × 65 mm), involving all cerebellar peduncles as well as the anterior aspect of the right cerebellar hemisphere extending further superiorly. There was additional interval increase in size of the lateral and third ventricles and cerebellar tonsillar descent below the foramen magnum (Fig. 1a.III). The patient remained on dexamethasone and received palliative care. He passed away 9 weeks after the last scan and the family generously donated his tumour via the QCTB.

Research autopsy was performed within hours of the patient's death and tissue annotated and banked. The tumour-infiltrated brainstem was segmented into ten cross-sections, including midbrain, pons, medulla and spinal cord (Fig. 1c). Formalin-fixed and paraffin-embedded (FFPE) tissue blocks were prepared for each of the ten samples and assessed for tumour burden. H&E staining demonstrated varying degrees of neoplastia, with high tumour observed in pontine regions and obvious signs of disease progression in the midbrain. The extent of DIPG tumour burden was confirmed via H3K27M immunohistochemistry (IHC) on matching FFPE tissue blocks (Fig. 1d and Supplementary Fig. S1c). RNA quality (DV200 values) was determined for all FFPE tissue blocks, confirming suitability of the samples for sequencing studies (Supplementary Fig. S1b).

Spatially informed cell type clustering highlights heterogeneous cell community distribution

Quality control and filtering was performed on each region individually (Supplementary Fig. S2a). To further compare the ten different brainstem regions and to identify conserved and shared features across all samples, the sequencing data from all samples was inferred via anchor-based data integration [21]. Visualisation of all the regions in Uniform Manifold Approximation and Projection (UMAP) confirmed successful data integration (Supplementary Fig. S2b). Unsupervised cell type clustering was performed on the integrated dataset, resulting in ten unique populations, herein referred to as cell communities (Fig. 2a and Supplementary Table S1). The ten communities represent all major brain cell types, including stem- and progenitor-like, glial, neuronal, myeloid and endothelial cell populations. We quantified the proportion of these further and showed that communities with an OPC/NPC (C0) and stem-like/glial (C1) phenotype were the predominant cell populations within our dataset (Fig. 2b). Considering the low resolution of the 10x Visium platform, we also performed subclustering on an example from cell community C0 to demonstrate that a more specific cell type identification is feasible for communities of interest. Further delineation of C0 revealed that this population is dominated by OPC-like cells, mixed with cancer stem-like NPCs and tumour-associated myeloid cells (Supplementary Fig. S3 and Supplementary Table S1). We next profiled the ten communities spatially, which showed a diffuse distribution of the different populations in all tissue regions (Fig. 2c). Liu et al. have previously analysed the spatial architecture of four H3 K27M DMG patient samples, performing IF-based co-detection by indexing (CODEX) [15]. Consistent with the results from this group, we found that the ten cell communities show varied distributions and clustering tendencies in a cell type-dependent manner. For instance, the OPC/NPC (C0) and stem-like/glial (C1) populations predominantly cluster with themselves, whereas other communities appeared to be more dispersed in the majority of the ten brainstem regions. This observation overall highlights the complex cellular heterogeneity present in this disease and suggests intercellular communication between the different cell populations.

Identification of tumour cell communities underlines co-existing DIPG subpopulations

Comprehensive sequencing studies from Suvà or Filbin and colleagues have identified the cellular origin and hierarchies underlying DMG tumourigenesis. Findings show that these tumours predominantly resemble cells of OPC and stem-like origin that give rise to more differentiated oligo- or astroglial populations [14, 15]. Hence,

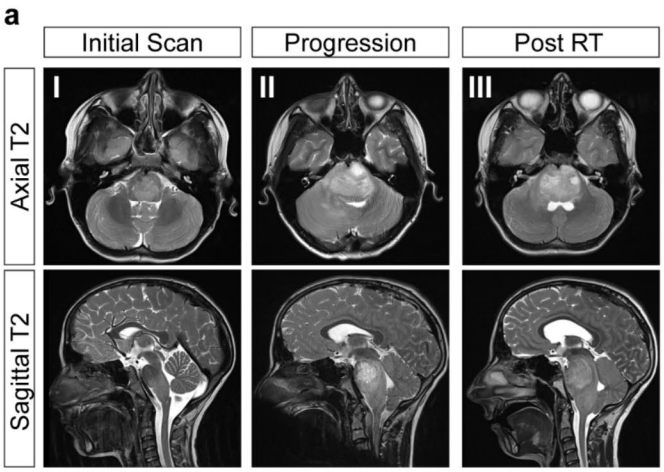

b

Gene Symbol	CDS Change	Amino Acid Change
H3F3A	c83.A>T	p.Lys28Met
TP53	c.818G>A	p.Arg273His
ATRX	c.5272T>A	p.Tyr1758Asn
PPM1D	c.126T>A	p.Ser421Ter
Chromosome	**Sequenza**	**Copy Number**
5q	Het	3
15q	Het	3
18	cnLOH	1

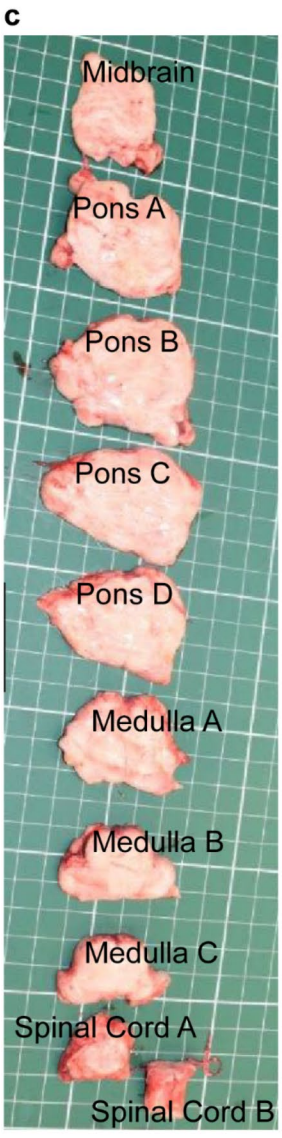

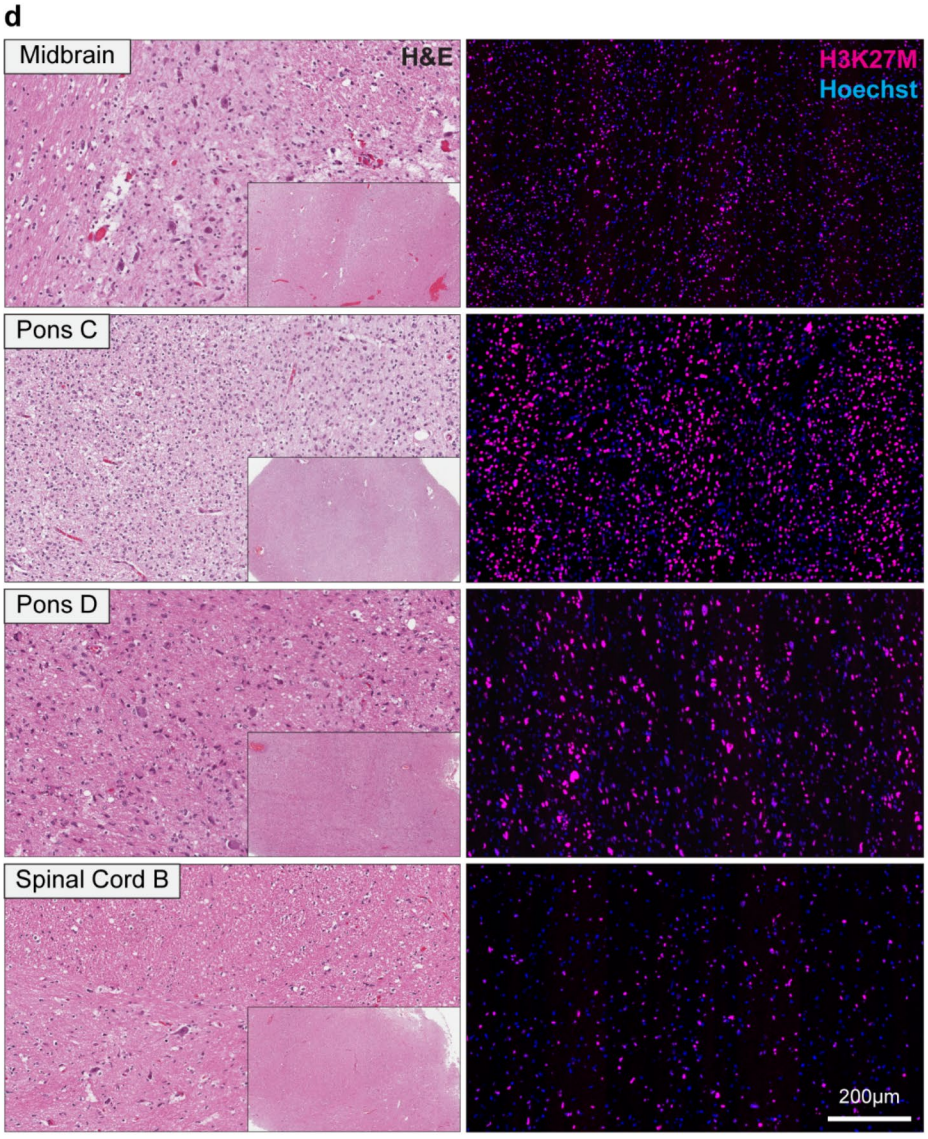

Fig. 1 Patient imaging and tumour characteristics. **a** MR images showing DIPG tumour progression over the course of disease. **b** Table summarising point mutations and chromosomal aberrations identified through tumour biopsy sampling and sequencing as part of the MNP2.0 (Germany) and PRISM (Sydney) trial. **c** Ten patient brainstem regions were collected at autopsy. **d** Different degrees of tumour burden were confirmed by H&E and H3K27M staining. Pontine regions showing areas of high cellularity, whereas the midbrain area shows clear patterns of tumour infiltration into normal brain tissue

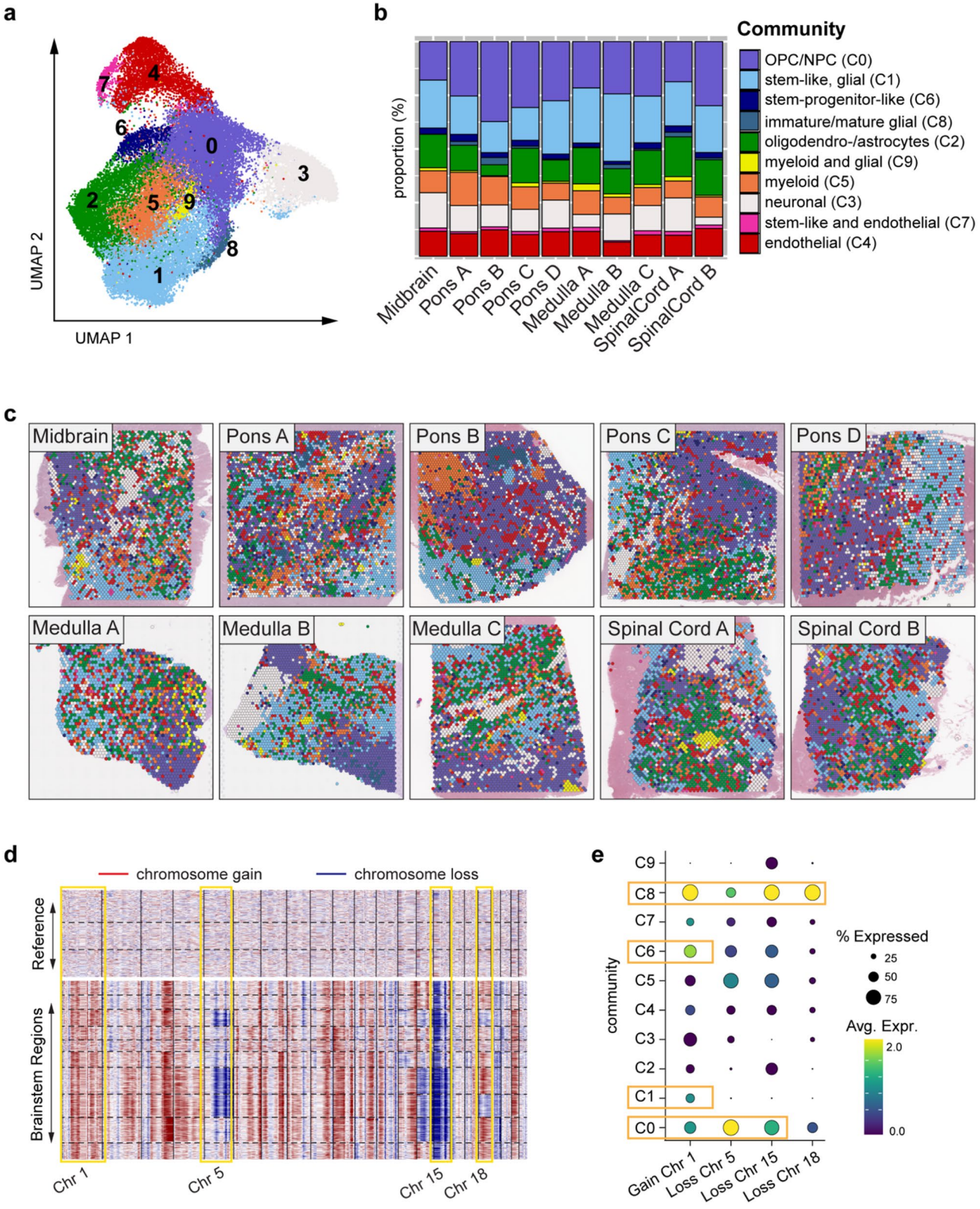

Fig. 2 (See legend on next page.)

(See figure on previous page.)

Fig. 2 Identification of DIPG cell communities. **a** UMAP plotting demonstrating unsupervised clustering and identification of ten distinct cell communities. **b** Quantification of all ten cell communities in all ten DIPG brainstem regions highlighting community C0 and C1 as the dominating populations. **c** Spatial visualisation of the ten cell communities in the brainstem regions showing heterogeneous distribution of the respective populations, including patterns of immune cell infiltration and highly compartmentalised OPC or stem-like populations. All major brain cell types are represented in the dataset. **d** InferCNV analysis was performed to identify chromosomal aberrations in the ten DIPG-infiltrated brainstem regions. 3 normal brain samples from SpatialLIBD were used as a control reference. Results demonstrated gain of chromosome 1, as well as losses of the chromosomes 5, 15 and 18 present in the spatial DIPG object. Loss of the chromosomes 5, 15, and 18 were previously identified via tumour biopsy sequencing (Fig. 1b). **e** Expression analysis of gain chr 1 and losses of chr 5, 15, 18 identified four communities with high levels of the chromosomal aberrations, including C0, C1, C6 and C8

it was reasonable to hypothesise that cell communities with OPC, NPC and stem-like phenotypes, in our dataset, represent DIPG cell populations. To assess this this computationally, we performed InferCNV, an established method to identify evidence for large-scale copy number variations (CNV) in single cell sequencing data [22]. The 10x Visium data generated here lacks single cell resolution, which makes the identification of normal cell types and accurate intereference of cell type-specific CNVs challenging. However, for this analysis, we further incorporated three normal, human dorsolateral prefrontal cortex (DLPFC) 10x Genomics Visium spatial transcriptomics datasets from spatialLIBD as a normal reference [23]. This approach was helpful to delineate 'higher tumour content' spots. Moreover, we incorporated single cell data from Filbin and colleagues to further corroborate our findings (discussed in more detail below). Amongst others, we found CNVs that were identified via biopsy sampling, including loss of chromosome (Chr) 5, 15 and 18. Analysis also determined gain of Chr1q, which is highly characteristic for DMG tumours [24] (Fig. 2d). To next determine which cell populations in our dataset represent a high proportion of DIPG tumour cells, we assessed the expression of the identified CNVs (gain chr1, loss chr 5, 15, 18) in the ten cell communities. Results confirmed that predominantly populations with an OPC and stem- or progenitor-like phenotype are associated with these aberrations. These included the strongly represented OPC/NPC (C0) and stem-like/myeloid (C1) cell communities, as well as the populations of C6 and C8 (Fig. 2e).

Tumour subpopulations reflect different DIPG cellular states

The identification of four distinct tumour cell communities suggested the presence of different DIPG subpopulations in our dataset [25, 26]. As aforementioned, previous work discovered that DIPG is comprised of numerous genetically and functionally distinct subclones that co-exist [14, 15, 26]. Following studies provided further evidence that these populations interact co-operatively to maintain tumourigenesis and promote DIPG development and progression in a spatiotemporal context [26–29]. We therefore sought to delineate patterns of heterogeneous tumour subpopulations in our dataset. For this approach, we integrated single cell data from a larger DMG cohort as a reference, looking at tumour cellular states and associated cell types [15]. We then performed conditional autoregressive-based deconvolution (CARD) to highlight malignant motives in our dataset [18]. Results clearly demonstrated a high presence of the AC-like phenotype across the specimens in all ten brainstem regions. This was followed by immune cells and cells with MES-like characteristics (Fig. 3a and Supplementary Fig. S4). Next, we focussed specifically on the four previously identified tumour communities, C0, C1, C6, C8, and assessed expression levels of selected marker genes associated with DIPG developmental programs in these populations. Results indicated that the four malignant populations indeed reflect distinct tumour clones. For instance, population C0 was associated with well-known DIPG marker genes, such as *NTRK2*, *EGFR*, or *OLIG2* (Fig. 3b). Specific profiling of DIPG cellular states confirmed that this population is correlated to the more committed OPC-like 1 and AC-like cellular state (Fig. 3c). Community C1, in turn, showed elevated stem cell and regulatory genes like *JUNB* and *FOS*, which assign to the more immature OPC-like 3 state [15]. This population also demonstrated a strong association with a MES-like phenotype. C8, which is represented to minor extent, correlated to both immature and more committed DIPG tumour cells, but harboured additional DNA damage response genes, such as *DDIT4*. Consistent with this observation, this population was most highly associated with the transitional OPC-like 2 state. Tumour population C6 was predominantly characterised by developmental and cell cycle genes, including *MKI67* or *CDC20* among others. However, in our analysis, no particular cell state was found to be correlated with this community. To explore the relationships between these tumour subpopulations further, we next performed spatial trajectory analysis. Supporting our hypothesis, results highlighted a trajectory tree from immature to more committed DIPG cells, proposing a transition from C6 to C1 to C8 to C0 (Fig. 3d and Supplementary Fig. S5). Hence, our findings strongly support previous data, describing the development from immature to more committed DIPG tumour cell populations and importantly, the presence of functionally distinct tumour niches in a spatiotemporal context. The overarching question therefore was whether such niches favour the occurrence of heterogeneous DIPG cell populations. To address this, we next examined

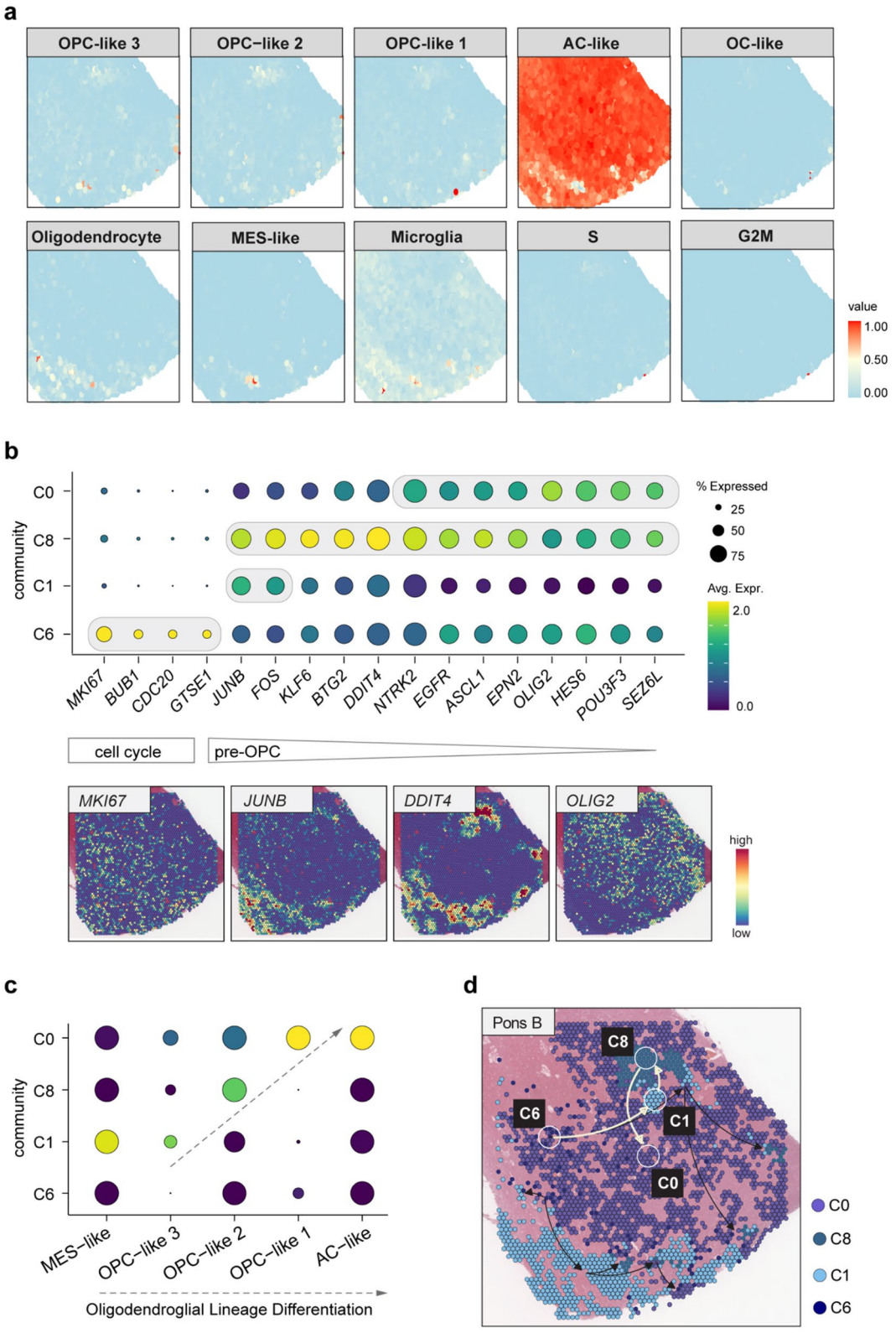

Fig. 3 (See legend on next page.)

(See figure on previous page.)

Fig. 3 Characterisation of DIPG tumour cell communities. **a** DIPG cellular states and tumour-associated cell types according to Liu et al. were assessed across the patient tissue at the spot-wise level. Reference-based deconvolution demonstrated a high degree of the AC-like phenotype in almost all communities. **b** The levels of selected marker genes associated with different DIPG cellular states were quantitated in the four tumour cell communities, demonstrating that C0 expresses known DIPG markers like *NTRK2* or *OLIG2*, whilst genes expressed in C1 are correlated with more immature populations such as *JUNB*. C8 appears to be a mix of C0 and C1, with additional DNA damage markers including *DDIT4*. Community C6 represents a rather unique population, expressing proliferation and cell cycle markers like *MKI67* and *CDC20*. **c** Signatures of DIPG cellular states were profiled more specifically across the four tumour cell communities, supporting the notion that these populations reflect different states of DIPG lineage differentiation. Community C1 shows characteristics of a more immature and MES-like state. C8 is associated with OPC-like 2 signatures whereas community C0 harbours characteristics of the more committed OPC-like 1 and AC-like cell state. **d** Spatial trajectory analysis was performed additionally to predict the trajectory path of the four tumour cell communities. Community C6, which is characterised by cell cycle markers such as *MKI67* was determined as the initiating cell population. Analysis confirmed previous results revealing that community C1 instigates the development of community C8 and C0

cellular interactions between the four different tumour populations and the TME.

DIPG tumour cells actively receive cues from endothelial, neuronal and myeloid cell populations

Gene expression profiling in the spatial context offers a significant opportunity to uncover important cell-cell or cell community interactions (CCIs). Information about known ligand-receptor (LR) pairs can be utilised to predict intercellular communication, based on the coordinated expression of genes in particular regions. We used stLearn to assess spatial neighbourhoods of LR co-expressions to compute corresponding LR scores in our dataset. We were then able to make inferences about cell community interactions. CCI scores were calculated for all ten cell communities and all ten brainstem regions respectively. (Supplementary Fig. S6a and Table S2). Interestingly, we observed clear differences between sender (ligand-expressing) and receiver (receptor-expressing) populations. For instance, the endothelial population was identified as the strongest interacting sender community. This was followed by two non-tumour communities, the neuronal and myeloid populations. Conversely, the tumour cell communities C1 and C0 were the most important receiver populations (Fig. 4a). These findings indicate that DIPG tumour cells actively receive cues from the TME and underline the importance of cellular communication, particularly between tumour, endothelial, neuronal and myeloid cell types.

Novel ligand-receptor candidates contributing to DIPG progression

To evaluate LR pairs involved in the above described CCIs, we first determined interacting partners involved in communication with all tumour cell communities combined, focussing on the three most significant interacting partners: endothelial-to-tumour, neuronal-to-tumour and myeloid-to-tumour. This was to identify those LR pairs that likely play a substantial role for the interaction between DIPG tumour cells and the TME globally (Fig. 4b and Supplementary Table S3). Endothelial-to-tumour interactions, identified *ENG-BMP2* (endoglin and bone morphogenic protein 2) as one significant, most frequently recurring LR pair. BMP2 belongs to the transforming growth factor-beta (TGF-β) family and has previously been associated with a glioma quiescent stem cell populations [30]. This is consistent with the vascular niche reflecting a known repository for glioma stem cells [31]. Gliomas further utilise the vascular niche to migrate along blood vessels and most recent studies on BMP2 suggest that signalling through this cell surface receptor promotes DIPG invasion [32]. Interaction profiling of neuronal-to-tumour communities highlighted *ADCYAP1-ADCYAP1R1* and *LGI1-ADAM23* as the most significant LR pairs. Previous work showed that Leucine-rich glioma inactivated 1 (LGI1) binding to the metalloproteinase ADAM23 regulates neuronal connectivity and morphology [33]. *ADCYAP1-ADCYAP1R1* encode for pituitary adenylate cyclase-activating polypeptide PACAP and the corresponding receptor PAC1. Notably, PACAP-PAC1-mediated cAMP/PKA was shown to regulate an invasive phenotype in adult GBM [34]. Lastly, we profiled immune-to-tumour interactions and found complement component C3 to be greatly involved in such communication, suggesting a possibly important role of this molecule to DIPG pathophysiology. Indeed, C3 has been demonstrated to alter a broad range of mitogenic signalling pathways in physiology and pathophysiology, including sustained oncogenesis, invasion and migration, angiogenesis or decreased apoptosis [35–39]. Crosstalk between myeloid cells and glioma cells via C3 were reported previously and a very recent study found that C3a-C3aR pairing between tumour-associated macrophages and glioma stem cells (GSCs) maintains the malignant phenotype of this population [40]. Additionally, we performed prediction analysis for selected LR pairs (*ENG-BMP2*, *ADCYAP1-ADCYAP1R1* and *C3-C3AR1*). Spatial profiling suggested that *ENG-BMP2* and *C3-C3AR1* interactions are strongly associated with the immature tumour community of C1, whereas *ADCYAP1-ADCYAP1R1* crosstalk was found in areas that are dominated by the more commited cell population C0 (Supplementary Fig. S6b).

Community-specific LR analysis suggests tumour population-specific mechanisms contributing to disease progression

Next, we specifically assessed the interaction profile for each tumour cell community respectively. Since the

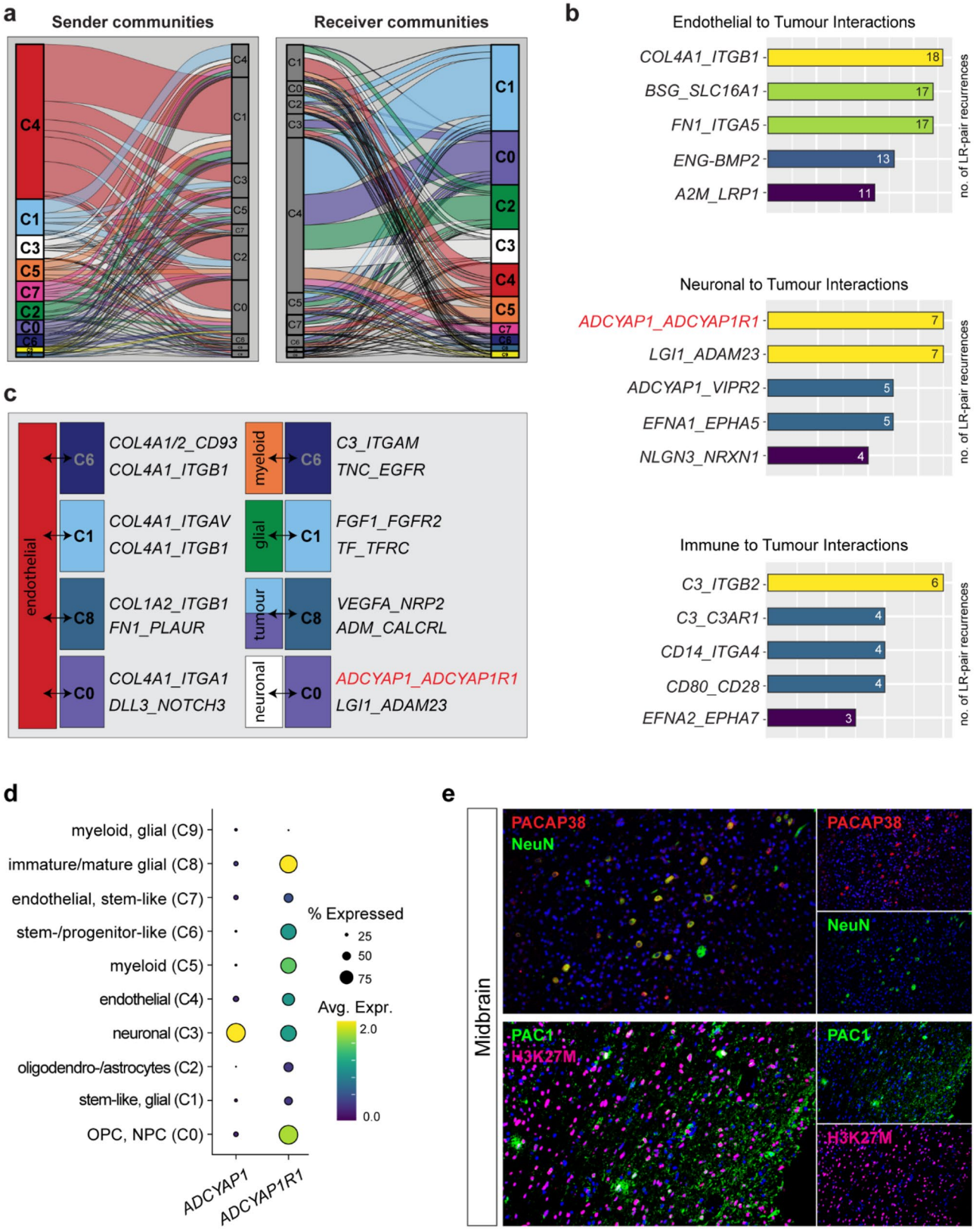

Fig. 4 (See legend on next page.)

(See figure on previous page.)

Fig. 4 Identification of CCIs and LR pairs. **a** Cell-cell interaction (CCI) scores were evaluated for each of the ten brainstem regions and between all ten cell communities. Sankey plotting highlighting the endothelial population as the top sender (ligand-expressing) community, followed by the two non-tumour populations of C3 (neuronal) and C5 (myeloid). The two most interacting receiver populations (receptor-expressing) identified by CCI profiling were the tumour communities C1 and C0. **b** The most significant ligand-receptor (LR) pairs involved in the crosstalk between the TME interaction partners identified in 5a (endothelial, neuronal and myeloid) and the four tumour communities combined were determined. **c** All four tumour populations were profiled to determine tumour subpopulation-specific LR pairs. Collagen and integrin pairs were identified as predominant endothelial-to-tumour interactions. Assessment of CCIs for each tumour population respectively revealed distinct results. C6 interacts mostly with myeloid cells, C1 with glial cells, C8 with the two tumour communities C0 and C1 and the more mature tumour sub-population of C0 interacts most strongly with neurons. **d** Assessment of *ADCYAP1* and *ADCYAP1R1* in the ten DIPG cell communities confirmed that expression of the ligand *ADCYAP1* is exclusive to the neuronal population, whereas *ADCYAP1R1* expression is most highly associated with the tumour cell communities of C0 and C8. **e** Immunohistochemistry staining of the corresponding proteins, PACAP38 and PAC1, on the same FFPE tissue blocks (Midbrain) confirmed this observation, showing co-expression of PACAP38 together with the neuronal marker NeuN and PAC1 expression predominantly on H3K27M positive DIPG cells

endothelial population was identified as the most significant sender community, we first focussed on interactions with this population. Members of the collagen and integrin family were consistently found to be the most important LR pairs across all four tumour populations. The contribution of cell-matrix interactions to glioma motility, stemness, survival and angiogenesis, including integrin-binding to collagens is established [41–43]. We further determined those populations that interact with each of the four tumour communities second most. Intriguingly, the interacting TME partners were different for each of the four tumour subpopulations. C6 interacted mostly with the myeloid population, C1 with glial cells, C8 with the tumour communities C1/C0, and C0 was found to communicate most strongly with the neuronal community (Fig. 4c and Supplementary Table S3). *TNC-EGFR* (tenascin-C and epidermal growth factor receptor), was found between myeloid cells and community C6. Notably, previous work demonstrated that tenascin-C levels influence immune response and microglial surveillance during cerebral ischemia [44]. Assessment of crosstalk between glial cells and the immature tumour community C1 identified *TF-TFRC* (transferrin and transferrin receptor) interactions. Iron uptake has been linked to tumour-initiating cells and maintenance of cancer stem cells and, encouraging our findings, transferrin has been shown to be expressed by mature oligodendrocytes whilst TF receptors are expressed on OPCs [45, 46]. Interaction profiling between tumour populations C8, C1 and C0 determined the LR pair adrenomedullin (ADM) and calcitonin receptors (CALCRL) to be highly involved in such communication. ADM binding to calcitonin receptors has been demonstrated to determine cell fate in neural stem cells [47]. Hence, not only the TME, but also different subpopulations of DIPG tumour cells regulate each other and drive lineage differentiation and development. Lastly, we again found *ADCYAP1-ADCYAP1R1* and *LGI1-ADAM23* interactions to be most highly involved in neuronal signalling towards the more committed population of C0. Our analysis therefore indicates that these communication axes play a considerable role for DIPG invasion. Shioda and colleagues demonstrated that PACAP-PAC1 interactions lead to increased calcium (Ca^{2+}) concentrations in rat neuroepithelial cells and downstream activation of the PLC/PKC (phospholipase C/protein kinase C) cascade [48]. The importance of Ca^{2+} signalling to modulate synaptic strength in DIPG is well established [49–51]. Hence, it is tempting to speculate that PACAP-PAC1 interactions contribute to neuron-to-glioma-mediated cell invasion in DIPG and that blocking this signalling pathway could provide a strategy to block synaptic communication. Intriguingly, the PACAP-mediated pathway has been implicated to play a notable role in chronic migraine and a phase II clinical trial (NCT04976309) targeting this neuropeptide is currently under investigation [52–54]. This finding is consistent with the body of evidence that neuron-to-glioma interactions crucially mediate glioma progression [55–59]. We therefore sought to investigate the expression of this pair further. Confirming our LR analysis, profiling of both genes in the ten cell communities respectively confirmed that ligand *ADCYAP1* is exclusive to the neuronal population. Expression of receptor *ADCYAP1R1* was found on the neuronal and myeloid communities to a certain extent, however it was most strongly associated with the more mature tumour cell communities C0 and C8 (Fig. 4d). To further substantiate our findings, we confirmed these observations at the protein level and performed immunohistochemistry (IHC) staining on the same FFPE tissue blocks. Dual staining for PACAP38, the corresponding protein for *ADCYAP1*, together with the neuronal marker NeuN confirmed expression of the ligand on neurons (Fig. 4e). Similarly, co-staining for PAC1, the corresponding protein for *ADCYAP1R1*, together with the DMG marker H3K27M demonstrated PAC1 expression on H3K27M positive cells. Lastly, we explicitly determined where interactions between this pair occur in the spatio-temporal context. Results suggest stronger communication in more distally located tumour regions, including Midbrain, Pons B and Medulla C. Spatially resolved assessment further demonstrated that such interactions largely appear to be locally restricted (Fig. 5a). Encouragingly, IHC staining for PACAP together with PAC1 supported our analysis, demonstrating PAC1-expressing cells surrounded by PACAP-positive cells, which were predominantly

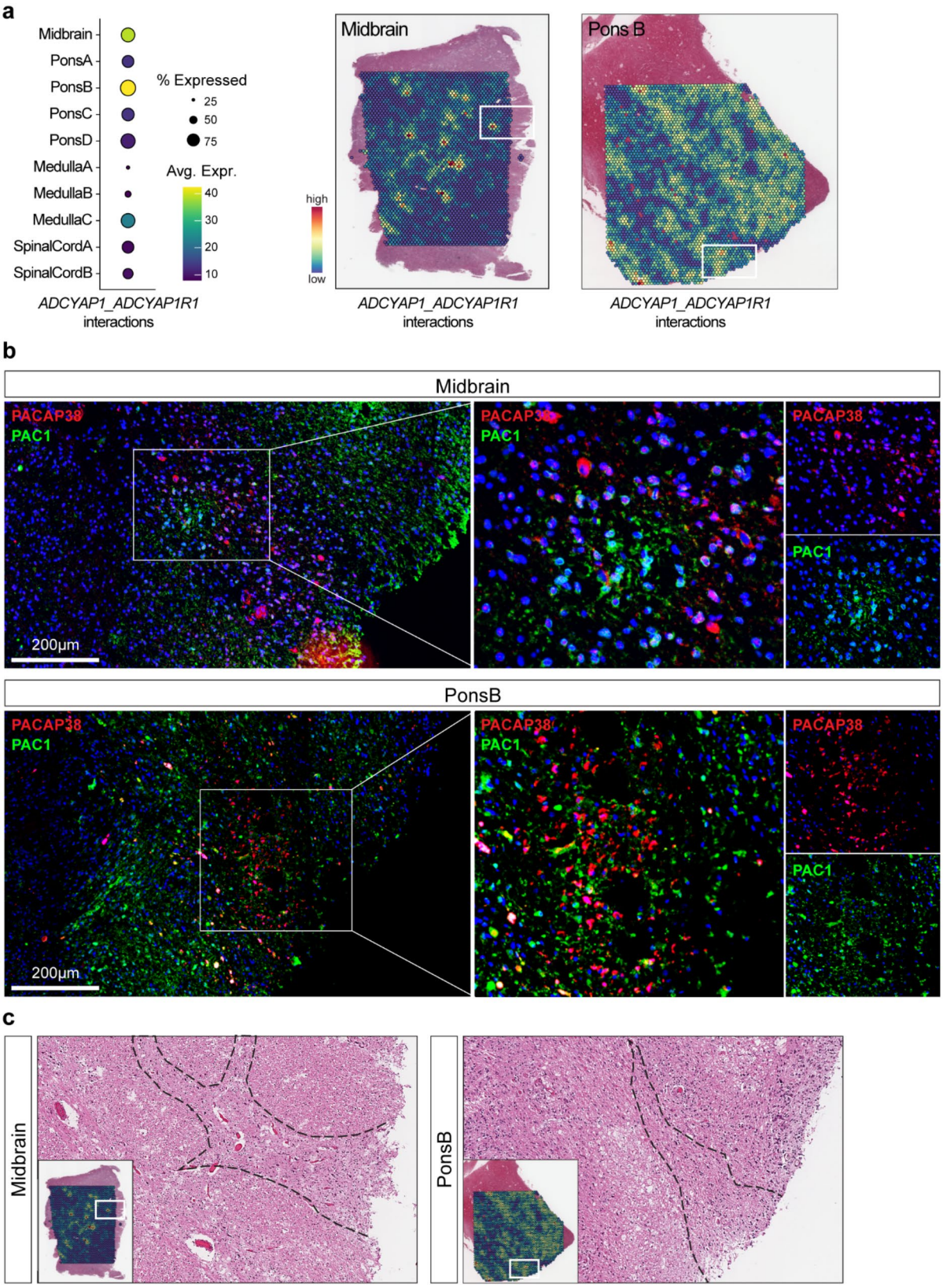

Fig. 5 *ADCYAP1-ADCYAP1R1* expression profiling. **a** Prediction analysis of interactions between the LR pair *ADCYAP1-ADCYAP1R1* demonstrating crosstalk between the pair more strongly correlated to the midbrain and distal pons/medulla regions. Spatial transcriptomic profiling showed that interactions between this LR pair are fairly restricted. **b** Dual IHC staining for the corresponding proteins, PACAP38 together with PAC1, further highlighted that PACAP38 expressing cells surround PAC1 positive cells. **c** These were predominantly found in areas that appear to show patterns of tumour cell infiltration

observed in regions that appear to show patterns of DIPG tumour cell infiltration on matching H&E sections (Fig. 5b and c).

Overall, our LR pair prediction analysis uncovers targetable candidates involved in these malignant processes and further highlights the importance of the vascular niche and the contribution of neuronal and myeloid cells to DIPG disease progression. Some of the LR pairs we identified are well known to promote pathophysiology in other disease settings and hence, interrupting these communication networks could prove useful to slow DIPG progression.

Discussion

Many sequencing studies of DIPG tumours have been conducted at the single cell and spatiotemporal level. However, complete profiling of an intact tumour-infiltrated brainstem from a DIPG patient has yet to be reported.

Our analysis uncovered four genetically diverse tumour cell populations that represent varying states of stemness and maturity, likely reflecting distinct tumour subclones [26, 28, 60]. Spatially-resolved studies from Ren as well as Filbin and colleagues suggested the presence of region-specific tumour niches that favour modes of tumour cell differentiation and the development of distinct tumour subclones [15, 61]. Spatial trajectory analysis in our dataset supported this notion. Thus, our findings and previous studies lend themselves to further investigation unravelling which molecular mechanisms directly promote such phenotype switches. Our spatially-resolved sequencing dataset offered such an opportunity and allowed us to study cellular communication between the heterogeneous cell populations, therefore speculating whether particular interactions between tumour cells and the TME promote the development of distinct subpopulations. Our CCI analysis highlighted tumour cells as the dominant receiver populations, clearly demonstrating that cancer cells extensively receive cues from neighbouring populations, rather than releasing such cues themselves. Not surprisingly, the vascular niche appears centrally involved in tumour-to-TME interactions, underscoring the importance of the tumour vascular bed for glioma growth and treatment resistance [62]. We also found that neuronal and myeloid cells strongly signal to tumour communities. Interestingly, neurons seem to interact more with tumour cells that are defined by known DIPG markers such as *NTRK2*, *EGFR* or *OLIG2*, whereas endothelial and myeloid populations seem to connect more to stem cell-like populations, marked by genes like *FOS* or *JUNB*. More importantly however, this analysis enabled us to identify specific ligand-receptor (LR) pairs that are involved in such cellular communication. PACAP-PAC1 is of particular note. This LR pair was most highly involved in neuron-to-tumour interactions in our dataset, but more interestingly, phase II clinical trials against both PACAP (NCT04976309) and PAC1 (NCT03238781) are under investigation for migraine prevention [53, 63]. This likely indicates that the respective compounds, both humanised monoclonal antibodies, demonstrate sufficient BBB penetration with low CNS toxicity. Hence, these drugs are readily available, paving the way for future functional in vitro and in vivo efficacy studies to explore whether disrupting this signalling axis could prove useful to reduce DIPG tumour spread.

In conclusion, spatially-resolved characterisation of DIPG holds significant potential to better understand underlying disease biology and to ultimately improve patient outcomes in this intractable disease setting. Our study suggested novel disease contributors that could be addressed therapeutically in future efforts to impede DIPG tumour progression. Although the 10x Visium approach lacks single cell resolution and additional multimodal studies should be conducted to further confirm our findings, this study provides useful and relevant information about DIPG in its entirety and our novel spatial dataset will hopefully inform future DIPG discovery and translational efforts.

Abbreviations

DIPG	Diffuse Intrinsic Pontine Glioma
DMG	Diffuse Midline Glioma
TME	Tumour Microenvironment
CNS	Central Nervous System
LR	Ligand-Receptor
CCI	Cell-Cell Interaction
OPC	Oligodendrocyte Precursor Cell
NPC	Neuronal Precursor Cell
CNV	Copy Number Variation
PACAP	Pituitary Adenylate Cyclase-Activating Polypeptide
PAC1	Pituitary Adenylate Cyclase-activating polypeptide type 1 receptor

Supplementary Information

The online version contains supplementary material available at https://doi.org/10.1186/s40478-025-01952-x.

Supplementary Material 1: Assessment of FFPE tissue blocks. a Schematic representation of the ten DIPG-infiltrated patient brainstem regions collected for this study. b Assessment of FFPE tissue quality demonstrating sufficient RNA quality for sequencing studies. Region Medulla A shows lowest RNA quality, whilst demonstrating tumour necrosis identified per H3K27M staining (c). c H&E and H3K27M staining confirming DIPG burden in all regions to varying degrees

Supplementary Material 2: Quality Control of sequenced DIPG tumour tissue regions. a Median counts and the mitochondrial gene content were assessed for each of the ten sequenced DIPG tissue regions respectively. Median counts ranging between 1,420 (Medulla A) and 30,695 (Pons B). The mitochondrial gene content was low for all tissue regions. b UMAP plotting showing dimensional reduction of the ten DIPG brainstem regions after merging and anchor-based data integration, confirming the data was successfully integrated for downstream analysis.

Supplementary Material 3: Cell type subclustering on an example from cell community C0. a UMAP representing the four subpopulations identified via Seurat's subclustering. Majority of C0 is comprised of OPC-like cells and tumour-associated macrophages. Cancer stem-like and NPC-like popula-

tions are represented only to a certain degree. b Spatial visualisation of the corresponding subclusters in the ten DIPG patient tissue samples confirming OPC-like populations and correlated immune cells are present across all tissue sections, whilst NPC-like cells are found in selected regions, including Pons B, Pons D and Spinal Cord B.

Supplementary Material 4: Cell state and cell type deconvolution in ten brainstem regions. Single cell data from Filbin and colleagues was used for conditional autoregressive-based deconvolution (CARD) and the expression of all phenotypes evaluated in the ten DIPG brainstem regions. Spatially-resolved visualisation highlighting the AC-like phenotype as the predominant population across all samples, followed by immune cells and MES-like characteristics. AC-like-high regions appear to correlate more strongly with cell community C0, whilst MES-like features seem to mostly overlap with the more immature community of C1.

Supplementary Material 5: Spatial trajectory analysis of tumour cell communities. a Spatial trajectory analysis was performed for all ten brainstem regions, predicting the trajectory of the four tumour cell communities. In all cases, a development from community C6 to C1 can be traced. A complete trajectory from C6 to C1 to C8 to C0 was observed in the regions Pons A, B and C, as well as in Medulla B and Spinal Cord A.

Supplementary Material 6: Cell-cell interaction profiling of the ten DIPG brainstem regions. a Cell-cell interaction (CCI) analysis was performed for all ten DIPG-infiltrated brainstem regions, assessing communication between the respective cell communities. The degree of CCIs differs across regions for most populations. The endothelial community C4 consistently dominates cellular communication in all DIPG-infiltrated brainstem regions. b Selected LR pairs shown in Fig 5b were examined in the spatial context. ENG-BMP2 interactions are widely distributed across the tissue, but associated with blood vessels as seen in the corresponding H&E. The endothelial community was predominantly found amid the immature tumour communities C1 and C6. The LR pair ADCYAP1-ADCYAP1R1, which was identified to be crucially involved in neuronal-to-tumour crosstalk, were found to be high in areas that show patterns of DIPG cell infiltration. These regions are dominated by the more immature tumour community C0. C3-C3AR1 interactions are more ubiquitous, but strongly represented in areas where myeloid and the immature tumour populations C6 and C1 are present.

Supplementary Material 7

Supplementary Material 8

Supplementary Material 9

Acknowledgements
We thank the Queensland Children's Tumour Bank (QCTB) for providing autopsy brain tissue samples and QIMR Berghofer Histology Core Facility for preparing paraffin embedded tissue blocks.

Author contributions
A.K., L.H., B.D and Q.N. conceptualisation; A.K. and U.B. processed autopsy patient tissue; A.K. and T.V. prepared samples for sequencing; A.K., O.M., X.T. and Q.N. data analysis; T.E.G.H. and M.K.M. provided patient autopsy tissue and pathology report; A.K. wrote the manuscript; L.H. and B.D. review and editing. All authors have reviewed the manuscript.

Funding
This study has been supported by generous donations from the Children's Hospital Foundation to the Children's Brain Cancer Centre (CBCC) and The Sid Faithfull Group to QIMR Berghofer.

Data availability
The processed spatial transcriptomic sequencing files generated in this study will be made available through the GEO database (GSE280990). All other files are available within the Supplementary Information provided with this paper.

Declarations

Ethical approval
This study was performed in line with ethical approval from the QIMR human research ethics (HREC) committee under project P3420.

Consent to publish
Written informed consent was obtained from the patient's legal representative. The authors affirm that human research participants provided informed consent for publication of the images in Figure(s) 1a and 1c.

Competing interests
The authors declare no competing interests.

Received: 31 October 2024 / Accepted: 9 February 2025
Published online: 19 February 2025

References

1. Bernstock JD et al (2024) Next-generation CAR T cell therapies for glioblastoma. Sci Transl Med 16(762):eadp2660
2. Venkataramani V et al (2022) Disconnecting multicellular networks in brain tumours. Nat Rev Cancer 22(8):481–491
3. Johung TB, Monje M (2017) Diffuse intrinsic pontine glioma: New Pathophysiological insights and emerging therapeutic targets. Curr Neuropharmacol 15(1):88–97
4. Warren KE et al (2012) Genomic aberrations in pediatric diffuse intrinsic pontine gliomas. Neuro Oncol 14(3):326–332
5. Monje M et al (2011) Hedgehog-responsive candidate cell of origin for diffuse intrinsic pontine glioma. Proc Natl Acad Sci 108(11):4453–4458
6. Bender S et al (2013) Reduced H3K27me3 and DNA hypomethylation are major drivers of gene expression in K27M mutant pediatric high-grade gliomas. Cancer Cell 24(5):660–672
7. Castel D et al (2015) Histone H3F3A and HIST1H3B K27M mutations define two subgroups of diffuse intrinsic pontine gliomas with different prognosis and phenotypes. Acta Neuropathol 130(6):815–827
8. Duchatel RJ et al (2019) Signal Transduction in diffuse intrinsic pontine glioma. Proteomics 19(21–22):1800479
9. Khuong-Quang DA et al (2012) K27M mutation in histone H3.3 defines clinically and biologically distinct subgroups of pediatric diffuse intrinsic pontine gliomas. Acta Neuropathol 124(3):439–447
10. Lapin DH, Tsoli M, Ziegler DS (2017) Genomic insights into diffuse intrinsic pontine glioma. Front Oncol, 7
11. Mackay A et al (2017) Integrated Molecular Meta-Analysis of 1,000 Pediatric High-Grade and diffuse intrinsic pontine glioma. Cancer Cell 32(4):520–537e5
12. Wu G et al (2012) Somatic histone H3 alterations in pediatric diffuse intrinsic pontine gliomas and non-brainstem glioblastomas. Nat Genet 44(3):251–253
13. Louis DN et al (2021) The 2021 WHO classification of tumors of the Central Nervous System: a summary. Neurooncology 23(8):1231–1251
14. Filbin MG et al (2018) Developmental and oncogenic programs in H3K27M gliomas dissected by single-cell RNA-seq. Science 360(6386):331–335
15. Liu I et al (2022) The landscape of tumor cell states and spatial organization in H3-K27M mutant diffuse midline glioma across age and location. Nat Genet 54(12):1881–1894
16. Kuleshov MV et al (2016) Enrichr: a comprehensive gene set enrichment analysis web server 2016 update. Nucleic Acids Res 44(W1):W90–W97
17. Pardo B et al (2022) spatialLIBD: an R/Bioconductor package to visualize spatially-resolved transcriptomics data. BMC Genomics 23(1):434
18. Ma Y, Zhou X (2022) Spatially informed cell-type deconvolution for spatial transcriptomics. Nat Biotechnol 40(9):1349–1359
19. Pham D et al (2023) Robust mapping of spatiotemporal trajectories and cell–cell interactions in healthy and diseased tissues. Nat Commun 14(1):7739
20. Efremova M et al (2020) CellPhoneDB: inferring cell–cell communication from combined expression of multi-subunit ligand–receptor complexes. Nat Protoc 15(4):1484–1506

21. Long Y et al (2023) Spatially informed clustering, integration, and deconvolution of spatial transcriptomics with GraphST. Nat Commun 14(1):1155
22. Erickson A et al (2022) Spatially resolved clonal copy number alterations in benign and malignant tissue. Nature 608(7922):360–367
23. Maynard KR et al (2021) Transcriptome-scale spatial gene expression in the human dorsolateral prefrontal cortex. Nat Neurosci 24(3):425–436
24. Warren KE et al (2011) Genomic aberrations in pediatric diffuse intrinsic pontine gliomas. Neurooncology 14(3):326–332
25. Nikbakht H et al (2016) Spatial and temporal homogeneity of driver mutations in diffuse intrinsic pontine glioma. Nat Commun 7(1):11185
26. Vinci M et al (2018) Functional diversity and cooperativity between subclonal populations of pediatric glioblastoma and diffuse intrinsic pontine glioma cells. Nat Med 24(8):1204–1215
27. Hoffman LM et al (2016) Spatial genomic heterogeneity in diffuse intrinsic pontine and midline high-grade glioma: implications for diagnostic biopsy and targeted therapeutics. Acta Neuropathol Commun 4:1
28. Nikbakht H et al (2016) Spatial and temporal homogeneity of driver mutations in diffuse intrinsic pontine glioma. Nat Commun 7:11185
29. Tari H et al (2022) Quantification of spatial subclonal interactions enhancing the invasive phenotype of pediatric glioma. Cell Rep 40(9):111283
30. Sachdeva R et al (2019) BMP signaling mediates glioma stem cell quiescence and confers treatment resistance in glioblastoma. Sci Rep 9(1):14569
31. Gilbertson RJ, Rich JN (2007) Making a tumour's bed: glioblastoma stem cells and the vascular niche. Nat Rev Cancer 7(10):733–736
32. Bruschi M et al (2024) Abstract 154: diffuse midline glioma invasion and metastasis rely on cell-autonomous signaling through a phenotypic switch controlled by BMP7. Cancer Res 84(6Supplement):154–154
33. Owuor K et al (2009) LGI1-associated epilepsy through altered ADAM23-dependent neuronal morphology. Mol Cell Neurosci 42(4):448–457
34. Bensalma S et al (2019) PKA at a cross-road of signaling pathways involved in the regulation of Glioblastoma Migration and Invasion by the neuropeptides VIP and PACAP. Cancers 11(1):123
35. Markiewski MM et al (2008) Modulation of the antitumor immune response by complement. Nat Immunol 9(11):1225–1235
36. Nozaki M et al (2006) Drusen complement components C3a and C5a promote choroidal neovascularization. Proc Natl Acad Sci U S A 103(7):2328–2333
37. Rutkowski MJ et al (2010) Cancer and the Complement Cascade. Mol Cancer Res 8(11):1453–1465
38. Tang Z et al (2009) C3a mediates epithelial-to-mesenchymal transition in proteinuric nephropathy. J Am Soc Nephrol 20(3):593–603
39. van Beek J et al (2001) Complement anaphylatoxin C3a is selectively protective against NMDA-induced neuronal cell death. NeuroReport 12(2):289–293
40. Zhang Y et al (2024) An NFAT1-C3a-C3aR positive feedback Loop in Tumor-Associated macrophages promotes a glioma stem cell malignant phenotype. Cancer Immunol Res 12(3):363–376
41. Bae E et al (2022) Integrin α3β1 promotes vessel formation of glioblastoma-associated endothelial cells through calcium-mediated macropinocytosis and lysosomal exocytosis. Nat Commun 13(1):4268
42. D'Abaco GM, Kaye AH (2007) Integrins: molecular determinants of glioma invasion. J Clin Neurosci 14(11):1041–1048
43. Payne LS, Huang PH (2013) The pathobiology of Collagens in Glioma. Mol Cancer Res 11(10):1129–1140
44. Manrique-Castano D et al (2021) Tenascin-C preserves microglia surveillance and restricts leukocyte and, more specifically, T cell infiltration of the ischemic brain. Brain Behav Immun 91:639–648
45. Leitner DF, Connor JR (2012) *Functional roles of transferrin in the brain.* Biochimica et Biophysica Acta (BBA) - General Subjects, 1820(3): pp. 393–402
46. Torti SV, Torti FM (2020) Iron and Cancer: 2020 vision. Cancer Res 80(24):5435–5448
47. Martínez-Herrero S et al (2012) Adrenomedullin as a growth and cell Fate Regulatory factor for adult neural stem cells, vol 2012. Stem Cells International, p 804717. 1
48. Zhou C-J et al (2001) PACAP activates PKA, PKC and Ca2 + signaling cascades in rat neuroepithelial cells. Peptides 22(7):1111–1117
49. Hongpaisan J, Alkon DL (2007) A structural basis for enhancement of long-term associative memory in single dendritic spines regulated by PKC. Proc Natl Acad Sci 104(49):19571–19576
50. Olds JL et al (1989) Imaging of memory-specific changes in the distribution of protein kinase C in the Hippocampus. Science 245(4920):866–869
51. Taylor KR et al (2023) Glioma synapses recruit mechanisms of adaptive plasticity. Nature 623(7986):366–374
52. Birk S et al (2007) The effect of intravenous PACAP38 on cerebral hemodynamics in healthy volunteers. Regul Pept 140(3):185–191
53. Rasmussen NB et al (2023) The effect of Lu AG09222 on PACAP38- and VIP-induced vasodilation, heart rate increase, and headache in healthy subjects: an interventional, randomized, double-blind, parallel-group, placebo-controlled study. J Headache Pain 24(1):60
54. Schytz HW et al (2008) PACAP38 induces migraine-like attacks in patients with migraine without aura. Brain 132(1):16–25
55. Pan Y et al (2021) NF1 mutation drives neuronal activity-dependent initiation of optic glioma. Nature 594(7862):277–282
56. Venkataramani V et al (2019) Glutamatergic synaptic input to glioma cells drives brain tumour progression. Nature 573(7775):532–538
57. Venkataramani V et al (2022) Glioblastoma hijacks neuronal mechanisms for brain invasion. Cell 185(16):2899–2917e31
58. Venkatesh HS et al (2015) Neuronal activity promotes Glioma Growth through Neuroligin-3 secretion. Cell 161(4):803–816
59. Venkatesh HS et al (2019) Electrical and synaptic integration of glioma into neural circuits. Nature 573(7775):539–545
60. Ryall ST et al (2018) Abstract 1184: clonal evolution of diffuse intrinsic pontine glioma. Cancer Res 78(13Supplement):1184–1184
61. Ren Y et al (2023) Spatial transcriptomics reveals niche-specific enrichment and vulnerabilities of radial glial stem-like cells in malignant gliomas. Nat Commun 14(1):1028
62. Jung E et al (2021) Tumor cell plasticity, heterogeneity, and resistance in crucial microenvironmental niches in glioma. Nat Commun 12(1):1014
63. Ashina M et al (2021) A phase 2, randomized, double-blind, placebo-controlled trial of AMG 301, a pituitary adenylate cyclase-activating polypeptide PAC1 receptor monoclonal antibody for migraine prevention. Cephalalgia 41(1):33–44

Publisher's note